Topological Defects in Flat Geometry: The Role of Density Inhomogeneity

Zhenwei Yao and Monica Olvera de la Cruz

Department of Materials Science and Engineering, Northwestern University, Evanston, Illinois 60208-3108, USA

(Received 5 June 2013; published 13 September 2013)

Topological defects are found in particles confined to planar disks interacting via the $1/r$ Coulomb potential. The total interior topological charge is found to monotonically converge to a negative value as the energy decreases during the relaxation process regardless of initial configurations; it is more negative in a larger cluster. The comparison with a uniform hyperbolic tessellation reveals an underlying hyperbolic structure in a low-energy configuration where the particle density increases from the center of the disk to its boundary. An elliptic structure is identified in an opposite particle distribution where the particle density decreases from the center to the edge of the disk. The novel mechanism of density inhomogeneity driven topological defects as well as the underlying geometric structure may shed light in understanding a wide variety of relevant systems.

DOI: 10.1103/PhysRevLett.111.115503 PACS numbers: 61.72.J−, 61.46.Bc, 61.72.Bb

Much has been learned in the last decade about the packing of particles on typical two-dimensional curved surfaces as a generalized Thomson problem, including spheres [1,2], tori [3–5], paraboloids [6], catenoid minimal surfaces [7,8], and other constant mean curvature surfaces [9]. The concept of the topological defect is a key in understanding the resulting patterns that are applicable to various systems, like the packing of virus capsids [10], cell division in bacteria [11], propagation of cracks [12], melting of two-dimensional materials [13–15], and frustration of colloidal crystals [1]. Most previous studies focused on the uniform distribution of particles. However, the distribution of mutually repelling particles confined on surfaces with boundaries via *a long-range potential* is generically inhomogeneous. Numerical simulations on nonuniform 2D Wigner crystals have been carried out for several interaction potentials using various simulation techniques [16–19]. These studies were mostly focused on the low-energy states of the system with less emphasis on the relaxation processes leading to the low-energy configurations. Robust behaviors of the system in relaxation processes may allow us to explore characteristic features of the true ground state. In addition, the understanding of the relation between density inhomogeneity and Gaussian curvature, whose role in frustrating crystalline order has been well established, is lacking.

To address these problems, we employ the simplest model system where like-charged particles are confined in a planar disk interacting via the $1/r$ Coulomb potential. The charge neutrality condition requires the existence of opposite charges; in our model, they are treated as frozen continuum background charges that do not influence the particle configurations. Experimental realizations of such a system could include electrons trapped in the surface of liquid helium, colloidal particles in organic solvents with large screening lengths, and charged nanoparticles adsorbed at oil-water interfaces [20–22]. We perform simulations to track the evolutions of 2D Coulomb clusters towards low-energy configurations due to the interplay of topological defects and density inhomogeneity. Our simulations show that although the resulting lattice is still locally triangular a twisted 2D hexagonal Wigner crystalline lattice fails to capture the inhomogeneous density distribution; topological defects inevitably emerge in the interior of the system, but with some regulation.

Specifically, we identify a quantity, the total interior topological charge Q_{int}, which converges monotonically to a negative constant accompanied energy reduction regardless of initial configurations in elusive evolutions of 2D Coulomb clusters. Furthermore, the negative sign of Q_{int} leads to a hyperbolic structure hidden in inhomogeneous low-energy particle configurations via a geometric mapping. And in opposite particle distributions where the particle density decreases from the center to the edge of the disk, an elliptic structure is identified. These structures in inhomogeneous systems can be attributed to the modification of length scales in comparison with the corresponding homogeneous systems. These metric modification induced topological defects are analogous to the introduction of topological defects by Gaussian curvature, which solely depends on the metric of the system according to the Gauss's Theorema Egregium [23]. The novel mechanism of inhomogeneity driven topological defects as well as the underlying hyperbolic and elliptic structures revealed in this work may shed light in understanding a wide variety of systems where entities with long-range interactions are confined to finite surfaces with fixed boundaries.

In our model the like-charged particles are confined in a planar disk interacting via the $1/r$ Coulomb potential. Given an initial configuration of particles labeled from 1 to N, we move the particle i by s along the direction of the force on it by all other particles. And we move a boundary particle according to the projection of the force on the

boundary. This procedure applies on all particles sequentially from $i = 1$ to N, and a new configuration of the particles is generated by a sweep over the whole system. Note that during a sweep only the movements that can reduce the energy of the system are accepted. The system is continuously updated by consecutive sweeps until the energy of the system cannot be reduced any more. In this force-driving protocol, the system evolves towards a low-energy state. We perform simulations with different initial conditions to obtain properties that are independent of initial conditions.

For a collection of particles scattered in a planar disk, bonds among them can be uniquely defined via the Delaunay triangulation. The topological charge of a vertex i (i.e., the particle i) is $q_i = 6 - z_i$ for an interior particle and $q_i = 4 - z_i$ for a particle at the boundary, where z_i is the coordination number of the particle i. The total topological charge of a topologically planar triangulated cluster is always 6, a topological invariant derived from the Euler characteristic of a disk [24]. We treat the topological defects as degrees of freedom rather than all the interacting particles so the number of degrees of freedom in the system is greatly reduced.

Figures 1(a) and 1(b) are two snapshots in the relaxation process of a Coulomb cluster where particles are initially randomly distributed within a disk of unit radius. The topological charges of vertices with five (red dots) and seven (blue dots) neighboring vertices are $+1$ and -1; they are the fivefold and sevenfold disclinations, respectively. A bounded pair of fivefold and sevenfold disclinations constitutes a dislocation. In the low-energy configuration in Fig. 1(b), the particles are more concentrated near the edge of the disk, and we find very rich defect structures. It is remarkable that isolated disclinations are also found in inhomogeneous particle distributions; they usually appear among particle arrays on curved substrates to topologically compensate the prevailing Gaussian curvature. In addition, the system abounds with isolated dislocations, linear scars (a charged chain of alternating fivefold and sevenfold disclinations), pleats (a neutral chain of dislocations), and compound defect clusters. The comparison of the state at $n_s = 25$ in Fig. 1(a) and the low-energy state in Fig. 1(b) shows the evolution of defects in the relaxation process, including the wiggle of the pleat in the left oval, the annihilation of defects in the lower circle and the approach of two dislocations via the glide of the upper dislocation in the right circle. The simulations show that these events facilitate the reduction of the energy.

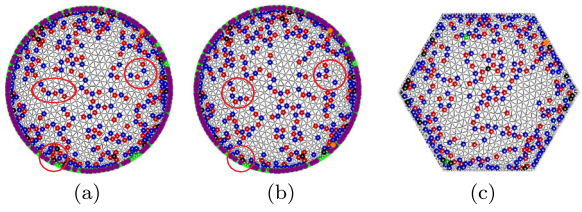

FIG. 1 (color online). (a),(b) The evolution of topological defects in the relaxation process of a two-dimensional Coulomb cluster starting from a random initial configuration. The number of sweeps is $n_s = 25$ (a) and $n_s = 37$ (b). (c) The low-energy configuration in a hexagonal disk. The coordination number $z = 3$ (purple), 4 (green), 5 (red), 7 (blue), 8 (black), and 9 (orange). $N = 1000$.

The evolution of individual topological defects in the whole relaxation process seems elusive. In order to find a pattern in this complicated process, we track the change of the total interior topological charge Q_{int}. Note that the planar topology of the system dictates a conserved total topological charge $Q_{\text{tot}} = Q_{\text{int}} + Q_{\text{boundary}} = 6$. Figure 2(a) summarizes the changes of different types of topological charges in the relaxation process starting from a random initial state. The total interior topological charge $Q_{\text{int}} = N_5 - N_7 + 2N_4 - 2N_8 + 3N_3 - 3N_9$, where N_i is the number of i-fold disclinations among interior particles. Figure 2(a) shows that the amount of all types of topological charges approaches some saturation value in the relaxation process. In particular, the value of the total interior topological charge Q_{int} monotonically converges to a negative constant -90, as read from the black dotted curves in Fig. 2(a). In simulation, we notice that the reduction of energy with the number of sweeps n_s follows a profile similar to that of Q_{int}. And the critical values of n_s at which the profiles of energy and Q_{int} become rather flat are also very close. The synchronic variation of the energy and the total interior topological charge implies a topological defects-mediated relaxation mechanism.

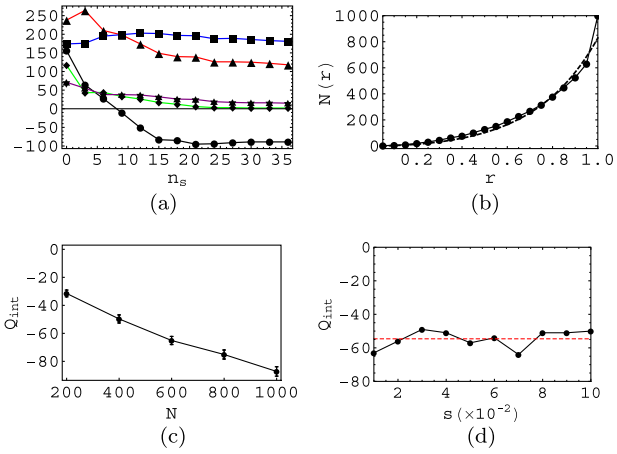

FIG. 2 (color online). (a) The topological charge vs the number of sweeps n_s in the relaxation of a Coulomb cluster. The diamonds, triangles, squares, and stars represent the number of fourfold (N_4), fivefold (N_5), sevenfold (N_7), and eightfold (N_8) disclinations in interior particles, respectively. The dotted black curve is for the total interior topological charge Q_{int}. (b) The cumulative particle distribution $N(r)$ vs r. $K_G = -12.7$ and $R_h = 1.05$. $N = 1000$ (a),(b). (c) Q_{int} vs the number of particles. The error bars show the slight variation of Q_{int} for ten independent initial configurations. (d) Q_{int} vs the step size s used in simulation, for a common initial configuration. $N = 500$.

To exclude the possibility that the observation of a negative Q_{int} in confined Coulomb clusters only applies to a particular initial configuration, we systematically study several systems with $N = 200$ to 1000, and for each system we start from several independent initial random configurations. It is found that the curves of Q_{int} vs n_s alway decline and converge to negative values, which is similar to the curve of Q_{int} vs n_s in Fig. 2(a). Figure 2(c) shows a linear relation between the total interior topological charge Q_{int} of the low-energy configurations and the number of particles, at least in the range of N from 200 to 1000. The value of Q_{int} is found to be more negative for a larger system. The error bars show the small standard deviation of Q_{int} for ten independent initial configurations, which indicates the robustness of the topological defect structure with constant Q_{int}. We further study how the step size s influences the value of Q_{int}, as shown in Fig. 2(d). The basic topological defect structure with negative Q_{int} is invariant using an alternative value for s, despite a fluctuation of as high as 9% relative to the mean value of Q_{int} according to the data in Fig. 2(d).

Considering that the number of metastable states proliferates exponentially with the number of particles, the identification of the ground state of the system is a great challenge. With high probability the low-energy configurations found in our simulations are not the true ground states. However, robust behaviors of the system like the smallness of the error bar in Fig. 2(c) imply that these low-energy configurations are at least close to the ground state. And they serve as a window to explore some characteristic features of the ground state.

It is natural to ask if the above observations rely on the incompatibility between the particular circular boundary and a perfect hexagonal lattice. In order to evaluate the influence of the boundary shape on the topological defect structure of the system, we adopt a hexagonal disk that is geometrically compatible with a hexagonal lattice and investigate if a deformed 2D hexagonal Wigner crystalline lattice can fit the low-energy configuration in this alternative boundary condition. Our simulations show that no qualitative change occurs in the hexagonal disk. Figure 1(c) shows a low-energy configuration in the hexagonal disk. The linear relation between Q_{int} and N still holds with only a slight change of the proportional constant. It indicates that it is the long-range interaction induced density inhomogeneity instead of a particular boundary shape that determines the basic topological defect structure.

It is interesting to identify the quantity Q_{int} from the elusive movements of mutually repelling particles towards a low-energy configuration; this quantity is always converging to a negative value in the relaxation process regardless of initial conditions. Recall that in uniform particle arrays on negatively curved surfaces negative topological charges appear as the response to the negative Gaussian curvature. We therefore expect a hyperbolic structure with negative Gaussian curvature hidden in the low-energy configuration of a Coulomb cluster. Note that the concept of conformal crystals, that is based on the elegant mathematical idea of conformal mapping from plane to plane, has been proposed to understand the bending of lattice lines towards the edge of the cluster as well as the density inhomogeneity [19,25]. It is interesting to interpret the topological defects observed in inhomogeneous systems from the perspective of the Gaussian curvature, whose role in inducing topological defects and frustrating crystalline order has been well established [24,25].

To extract the underlying hyperbolic structure, we introduce the Poincaré disk model, which is a conformal mapping from a hyperbolic plane to a finite planar disk. The triangular lattice is preserved in conformal mappings. In our case, the planar disk of radius R where the particles are confined is inversely mapped to a *finite* hyperbolic disk of radius R_h. The planar disk is therefore part of a complete Poincaré disk. The metric tensor in the planar disk of radius R is given in

$$ds^2 = 4\left(\frac{R}{R_h}\right)^2 \frac{dx^2 + dy^2}{[1 + K_G(x^2 + y^2)]^2}, \tag{1}$$

where x and y are the Cartesian coordinates, $K_G < 0$ is the Gaussian curvature of the hyperbolic disk with geodesic radius R_h, and the prefactor $(R/R_h)^2$ describes the uniform shrinking of the system. Figure 3 shows a schematic plot of the inhomogeneous particle configuration in a complete Poincaré disk corresponding to a uniform distribution of particles in an infinite hyperbolic plane; the particles away from the center are more squeezed, which is similar to the configuration in Fig. 1(b). By making use of the expression $A(r) = 4\pi(1/|K_G|)\sinh^2((1/2)\sqrt{-K_G}r)$ for the area of a hyperbolic circle of geodesic radius r, we derive the number of particles within the circle of radius r in the planar disk:

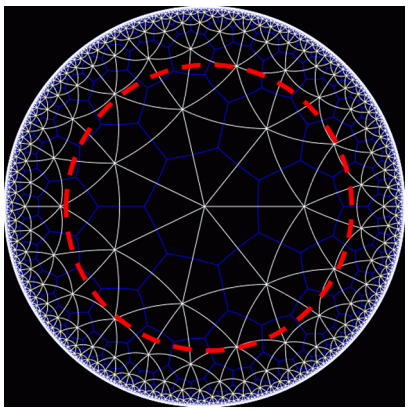

FIG. 3 (color online). A {3, 7} uniform hyperbolic tessellation shown in the Poincaré disk. Seven regular "three gons"surround each vertex. The dashed part schematically corresponds to the planar disk where particles sit in our system. Courtesy Don Hatch [31].

$$N_{\text{hyperbolic}}(r; R_h, K_G) = N\frac{\sinh^2(\frac{1}{2}\frac{xr}{R})}{\sinh^2(\frac{1}{2}x)}, \quad (2)$$

where $x = \sqrt{-K_G}R_h$. It will be shown later that, as a first order approximation, it is sufficient to treat the Gaussian curvature as a constant in order to reach an agreement between the analytical result and the simulation data.

The parameter K_G in Eq. (2) can be determined by the total interior topological charge Q_{int} of the corresponding low-energy configuration in simulations. From the balance of the topological charges and the total Gaussian curvature [8], i.e., $K_G A(R_h) = -(\pi/3)Q_{\text{int}}$, we obtain $K_G = -\pi Q_{\text{int}}/(3A(R_h))$. Since $A(R_h)$ depends on K_G, we numerically solve for K_G to feed the expression for $N_{\text{hyperbolic}}(r; R_h, K_G)$. Figure 2(b) shows the cumulative particle distribution $N_{\text{hyperbolic}}$ (dashed curves) and that of the corresponding low-energy configuration in Fig. 1(b) (solid curves). Their agreement suggests a hyperbolic structure in the low-energy configuration in Coulomb clusters; a certain amount of negative topological charge is required to compensate the underlying negative Gaussian curvature. The slightly faster increase of the solid curve in Fig. 2(b) in comparison with the dashed one indicates a more negative Gaussian curvature in the small region near the edge of the disk; this slight modification of the Gaussian curvature does not alter the hyperbolic nature of the underlying geometric structure. The idea of mapping an inhomogeneous particle configuration to a homogeneous copy behind Eq. (2) can be generalized to deal with other relevant inhomogeneous systems. Therefore, one is able to use sophisticated methods that have already been developed for homogeneous systems.

We further investigate if there is an elliptic structure with constant Gaussian curvature in a configuration where the particle density decreases towards the boundary. In order to generate such a density profile, we apply a constant centripetal force on each particle so the whole cluster is uniformly compressed; i.e., the whole system is placed in a conelike external potential. Figures 4(a) and 4(b) are two low-energy

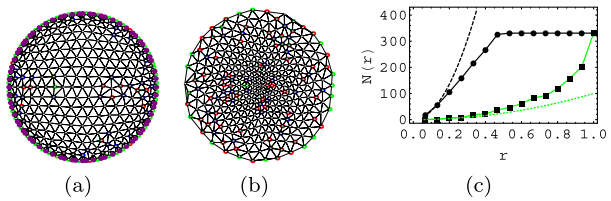

FIG. 4 (color online). (a),(b) The low-energy configurations of a Coulomb cluster under compression. A larger centripetal force is applied in (b) than in (a). $N = 331$. $R = 1$. (c) The cumulative particle distribution $N(r)$ in the compressed low-energy configurations for the configuration in (a) (squared, green) and in (b) (dotted, black). The dashed quadratic curves represent uniform distribution of particles. The flat part of the dotted black curve is indicative of the separation of the cluster from the circular boundary in the compression process.

states in the compression process starting from the initial configuration where a perfect hexagonal lattice is inscribed by the circular boundary of the disk. The compression of the cluster reverses the particle distributions, as shown in Fig. 4(c). The lower solid curve (in green) in Fig. 4(c) corresponds to the configuration in Fig. 4(a) and the upper solid curve (in black) to Fig. 4(b). For a uniform distribution of particles, $N(r) \sim r^2$. With the reversal of the particle density distribution, the value of Q_{int} switches from a negative value [$Q_{\text{int}} = -60$ in Fig. 4(a)] to a positive value [$Q_{\text{int}} = +20$ in Fig. 4(b)]. Note that positive Q_{int} is also observed in Coulomb clusters where the particles are more concentrated near the center of the cluster due to a circular parabolic external potential using minima hopping simulations [26] and the Metropolis simulated annealing algorithm [19]. These external physical potentials are corresponding to a positive Gaussian curvature; both tend to induce positive topological defects. In this sense, a physical potential gains a geometric interpretation.

The strong coupling between density inhomogeneity and topological defect structure is therefore disclosed. This coupling is mediated by the Gaussian curvature. The Gaussian curvature solely depends on the metric of the system according to Gauss's Theorema Egregium [23]. Consequently, the change of the metric, i.e., the change of the distance between particles in deforming homogeneous particle arrays on a flat geometry to an inhomogeneous configuration leads to the change of the Gaussian curvature from zero (for homogeneous density in flat geometry) to a nonzero value. It is the nonvanishing underlying Gaussian curvature that impairs the crystalline order in inhomogeneous particle arrays, which is similar to the frustration of crystalline order by the explicit Gaussian curvature of the curved surface where the particles are embedded. In relaxation processes, as a response to the metric modification, topological defects can be squeezed out by the rearrangement of bonds even if the particles are in a planar disk with vanishing Gaussian curvature. Because of the interplay of topological defects and density inhomogeneity, the system evolves towards a low-energy configuration.

In summary, we identify the total interior topological charge Q_{int} that converges to some constant in the elusive relaxation of a Coulomb cluster. The negative sign of Q_{int} leads to a hyperbolic structure underlying in the Coulomb cluster model; it originates from the modification of local length scales by either the long-range potential between particles or external potentials. The coupling between topological defect structures and inhomogeneous particle density as studied in this work can shed light in understanding intriguing behaviors in a wide variety of long-range interacting systems [27]. It includes the open question of the melting scenario in systems with long-range potentials, and the recently observed highly coupled dynamics of topological defects and the fluctuation of local

densities [28] in a wide variety of collectively moving particles like flocks of birds [29] and bacteria [30].

This work was funded by grants from the Office of the Director of Defense Research and Engineering (DDR&E) and the Air Force Office of Scientific Research (AFOSR) under Award No. FA9550-10-1-0167. Z. Y. would like to thank Rui Zhang and Rastko Sknepnek for many stimulating discussions on the Coulomb cluster system.

[1] A. Bausch, M. Bowick, A. Cacciuto, A. Dinsmore, M. Hsu, D. Nelson, M. Nikolaides, A. Travesset, and D. Weitz, Science **299**, 1716 (2003).
[2] M. Bowick, H. Shin, and A. Travesset, Phys. Rev. E **75**, 021404 (2007).
[3] L. Giomi and M. J. Bowick, Phys. Rev. E **78**, 010601 (2008).
[4] E. Pairam and A. Fernandez-Nieves, Phys. Rev. Lett. **102**, 234501 (2009).
[5] Z. Yao and M. J. Bowick, Eur. Phys. J. E **34**, 1 (2011).
[6] L. Giomi and M. Bowick, Phys. Rev. B **76**, 054106 (2007).
[7] W. Irvine, V. Vitelli, and P. Chaikin, Nature (London) **468**, 947 (2010).
[8] M. Bowick and Z. Yao, Europhys. Lett. **93**, 36 001 (2011).
[9] H. Kusumaatmaja and D. J. Wales, Phys. Rev. Lett. **110**, 165502 (2013).
[10] D. Caspar and A. Klug, in *Cold Spring Harbor Symposia on Quantitative Biology* (Cold Spring Harbor Laboratory Press, New York, 1962), Vol. 27, p. 1.
[11] D. Pum, P. Messner, and U. Sleytr, J. Bacteriol. **173**, 6865 (1991).
[12] M. J. Buehler, *Atomistic Modeling of Materials Failure* (Springer, New York, 2008).
[13] D. R. Nelson and B. I. Halperin, Phys. Rev. B **19**, 2457 (1979).
[14] J. Kosterlitz and D. Thouless, J. Phys. C **6**, 1181 (1973).
[15] A. Radzvilavičius, Phys. Rev. E **86**, 051111 (2012).
[16] V. M. Bedanov and F. M. Peeters, Phys. Rev. B **49**, 2667 (1994).
[17] Y.-J. Lai and I. Lin, Phys. Rev. E **60**, 4743 (1999).
[18] M. Kong, B. Partoens, A. Matulis, and F. M. Peeters, Phys. Rev. E **69**, 036412 (2004).
[19] A. Mughal and M. A. Moore, Phys. Rev. E **76**, 011606 (2007).
[20] M. W. Cole, Rev. Mod. Phys. **46**, 451 (1974).
[21] A. Yethiraj and A. van Blaaderen, Nature (London) **421**, 513 (2003).
[22] K. Larson-Smith, A. Jackson, and D. Pozzo, Langmuir **28**, 2493 (2012).
[23] B. Audoly and Y. Pomeau, *Elasticity and Geometry* (Oxford University Press, Oxford and New York, 2010).
[24] D. Nelson, *Defects and Geometry in Condensed Matter Physics* (Cambridge University Press, Cambridge, England, 2002).
[25] A. Mughal and D. Weaire, Proc. R. Soc. London, Ser. A **465**, 219 (2009).
[26] A. Radzvilavičius and E. Anisimovas, J. Phys. Condens. Matter **23**, 385301 (2011).
[27] *Long-Range Interacting Systems*, edited by T. Dauxois and L. Cugliandolo (Oxford University Press, Oxford, 2008).
[28] V. Schaller and A. R. Bausch, Proc. Natl. Acad. Sci. U.S.A. **110**, 4488 (2013).
[29] M. Ballerini *et al.*, Proc. Natl. Acad. Sci. U.S.A. **105**, 1232 (2008).
[30] C. Dombrowski, L. Cisneros, S. Chatkaew, R. E. Goldstein, and J. O. Kessler, Phys. Rev. Lett. **93**, 098103 (2004).
[31] http://www.plunk.org